Acoustic attenuation compensation in photoacoustic tomography using time-variant filtering

Bradley E. Treeby

Acoustic attenuation compensation in photoacoustic tomography using time-variant filtering

Bradley E. Treeby
University College London, Department of Medical Physics and Bioengineering, Gower Street, London WC1E 6BT, United Kingdom

Abstract. Most reconstruction algorithms used in photoacoustic tomography do not account for the effects of acoustic attenuation on the recorded signals. For experimental measurements made in biological tissue, the frequency dependent acoustic attenuation causes high frequency components of the propagating photoacoustic waves to be significantly reduced. This signal loss manifests as a depth dependent magnitude error and blurring of features within the reconstructed image. Here, a general method for compensating for this attenuation using time-variant filtering is presented. The time-variant filter is constructed to correct for acoustic attenuation and dispersion following a frequency power law under the assumption the distribution of attenuation parameters is homogeneous. The filter is then applied directly to the recorded time-domain signals using a form of nonstationary convolution. Regularization is achieved using a time-variant window where the cutoff frequency is based on the local time-frequency distribution of the recorded signals. The approach is computationally efficient and can be used in combination with any detector geometry or reconstruction algorithm. Numerical and experimental examples are presented to illustrate the utility of the technique. Clear improvements in the magnitude and resolution of reconstructed photoacoustic images are seen when acoustic attenuation compensation is applied. © *2013 Society of Photo-Optical Instrumentation Engineers (SPIE)* [DOI: 10.1117/1.JBO.18.3.036008]

Keywords: photoacoustics; acoustic absorption; attenuation compensation; time-variant filtering; nonstationary convolution.

Paper 130028R received Jan. 21, 2013; revised manuscript received Feb. 19, 2013; accepted for publication Feb. 20, 2013; published online Mar. 14, 2013.

1 Introduction

Photoacoustic tomography is a rapidly emerging biomedical imaging technique based on the generation of ultrasound waves within soft tissue through the absorption of pulsed laser light.[1,2] The ultrasound waves are generated when photons are absorbed by tissue chromophores, which thermalize the absorbed optical energy to create a local increase in temperature and pressure.[3] The increase in pressure then propagates outward as an acoustic wave. To create a photoacoustic image, the temporal evolution of this pressure field is sampled using an array of ultrasound detectors placed on the tissue surface. Images of the initial pressure distribution within the tissue are then reconstructed by solving an inverse source problem.[4]

The ultrasound waves generated in photoacoustics are usually very broadband with energy at frequencies from hundreds of kilohertz to many tens of megahertz.[5,6] As these waves propagate to the tissue surface where they are detected, some of this acoustic energy is lost to random thermal energy due to acoustic absorption. The exact mechanisms for this absorption are complex and occur at both the cellular level (e.g., viscous relative motion and thermal conduction) and the molecular level (e.g., molecular and chemical relaxation).[7,8] Additional acoustic energy is also lost due to scattering. This is generally negligible at low megahertz frequencies[9] but can become significant as the wavelength decreases.[10] In soft tissue, the overall acoustic attenuation (which includes both absorption and scattering) has been experimentally observed to follow a frequency power law.[11]

The effect of this frequency-dependent acoustic attenuation on photoacoustic images is a depth-dependent blurring or loss of resolution. These effects were first noted shortly after experimental photoacoustic systems began to appear in the late 1990s,[12] and they have since been studied by a number of authors.[13–16] For a given measurement sensitivity, the attenuation dictates the maximum frequency that can be detected from a broadband photoacoustic source located at a particular depth within the tissue.[6] This in turn dictates the maximum achievable resolution in the reconstructed image.[16] The effects of attenuation also remain noticeable when narrow-band transducers are used to detect the photoacoustic signals.[17] The compensation of acoustic attenuation is therefore important for improving the resolution of photoacoustic images, in addition to obtaining quantitatively accurate reconstructions of the initial pressure distribution.[18] Though a number of approaches for compensating for acoustic attenuation in photoacoustic tomography have been suggested, attenuation compensation is still not widely used by the photoacoustic community. Here, a general framework for compensating for acoustic attenuation in photoacoustic tomography is proposed based on the idea of time-variant filtering. This approach is straightforward to implement and does not depend on the experimental geometry or reconstruction algorithm used.

2 Background and Theory

2.1 Acoustic Attenuation in Tissue

The acoustic attenuation within soft biological tissue over the frequency range of interest in biomedical photoacoustics has

Address all correspondence to: Bradley E. Treeby, University College London, Department of Medical Physics and Bioengineering, Gower Street, London WC1E 6BT, United Kingdom. Tel: +44 20 7679 0249; E-mail: b.treeby@ucl.ac.uk

been experimentally shown to follow a frequency power law of the form[11]

$$\alpha = \alpha_0 \omega^y, \qquad (1)$$

where α is the acoustic attenuation in Np m^{-1}, α_0 is the power law prefactor in Np (rad/s)$^{-y}$ m^{-1}, ω is the angular frequency in rad/s, and y is the power law exponent, which is typically between 1 and 2. As a consequence of causality, acoustic attenuation is accompanied by sound speed dispersion (a dependence of the sound speed or phase velocity on frequency). This causes broadband waves to change shape as they propagate.[19] The frequency dependence of the attenuation and dispersion are connected by the Kramers-Kronig relations.[20] For power law attenuation of the form given by Eq. (1) with $0 < y < 3$ and $y \neq 1$, the frequency dependence of the sound speed is governed by[21]

$$\frac{1}{c_2(\omega_2)} - \frac{1}{c_1(\omega_1)} = \alpha_0 \tan(\pi y/2)(\omega_2^{y-1} - \omega_1^{y-1}), \qquad (2)$$

where $c_1(\omega_1)$ and $c_2(\omega_2)$ are the sound speeds in ms^{-1} at two different frequencies ω_1 and ω_2. A general dispersion relation between the spatial wavenumber $k(\omega)$ and the temporal frequency ω that satisfies both Eqs. (1) and (2) can be written as[22]

$$k(\omega) = \frac{\omega}{c_0} + i\alpha_0|\omega|^y + \alpha_0 \omega |\omega|^{y-1} \tan(\pi y/2), \qquad (3)$$

where c_0 is the isentropic sound speed [the dispersion relation for Szabo's wave equation can be derived as a special case of Eq. (3) by squaring this relation and discarding $O(\alpha_0^2)$ terms[23,24]]. This can then be used to define a lossy wave equation of the form

$$[\nabla^2 + k^2(\omega)]p = 0, \qquad (4)$$

for which the lossy Green's function is given by

$$G(d,\omega) = \frac{e^{ik(\omega)d}}{4\pi d} = \frac{e^{i\omega d/c_0}}{4\pi d} e^{-\alpha_0 d[|\omega|^y - i \tan(\pi y/2)\omega|\omega|^{y-1}]}, \qquad (5)$$

where d is the distance between the source and receiver in units of m. The first exponential term in the final expression in Eq. (5) is the normal three-dimensional free-space Green's function for the lossless linear wave equation. The second exponential term describes the attenuation and dispersion of acoustic waves in a lossy medium, in this case with power law attenuation and dispersion. The task in attenuation compensation is to reverse or counteract the effects of this second term. Since this is dependent on both frequency and time (where $t = d/c_0$), attenuation compensation cannot be achieved via simple linear filtering.

2.2 Attenuation Compensation in Photoacoustic Tomography

A simple approach for attenuation compensation is to apply a frequency domain filter of the form $e^{\alpha_0|\omega|^y d}$ to each of the recorded time series before image reconstruction, where the distance d is fixed and chosen in advance (removing the dependency of the filter on both t and ω). This was first discussed by Tan et al.,[25] who demonstrated a general improvement in image resolution after attenuation compensation using experimental

measurements of a turbid gel phantom with three small hairs located in the central region. A similar approach has recently been used for attenuation compensation when photoacoustic waves propagate through an absorbing layer of known thickness.[15,26,27] However, since d is fixed, this procedure is not suitable when the image features are positioned in an absorbing medium at varying distances from the receiver (as is most often the case in practice). In this case, signals arising from features shallower than the chosen d will be overcompensated, and signals from deeper features will be undercompensated.

A more general approach for attenuation compensation was proposed by La Rivière et al., in which the time-varying pressure signals p_{att} measured at the tissue surface are related to the equivalent unattenuated (or corrected) signals p via an integral relation of the form $p_{att} = Lp$.[28,29] The original form of the operator L was derived by relating p and p_{att} in the temporal frequency domain using a lossy wave equation proposed by Szabo that accounts for power law absorption.[23,30] (This derivation is repeated in general form in the Appendix.) Attenuation compensation can then be achieved by forming a matrix equation and computing the inverse of L to calculate an estimate of p from p_{att}. However, in general, the integral equation $p_{att} = Lp$ is not well conditioned, which makes this inversion ill-posed.[31,32] In the original, a regularized pseudoinverse of L was computed via singular value decomposition (SVD) by thresholding the eigenvalues.[28] To improve the stability of the inversion, Ammari et al. later suggested an asymptotic form of L for small α_0 that can be more easily inverted using a recursive scheme.[33] Kowar and Scherzer discussed a similar formulation to La Rivière for a range of other lossy wave equations and provided an analysis of the ill-conditioning of the integral equations via SVD.[32]

In a slightly different approach, Modgil et al. derived an integral equation relating the measured pressured signals p_{att} directly to the reconstructed initial pressure distribution p_0 (including attenuation compensation) assuming a planar detection geometry.[34–36] The corresponding matrix equation was again inverted using truncated-SVD. In this case, the smaller eigenvalues were shown to correspond to wavelet-like eigenvectors with their energy concentrated deeper into the tissue. This is consistent with the expectation that high frequencies generated by deeper features in the tissue are more difficult to recover. Kowar provided similar integral relations relating p_{att} to p_0 for point, line, and planar detectors in simple geometries based on a variant of Szabo's equation satisfying more stringent causality requirements.[37] These approaches have not yet been applied to experimental photoacoustic data.

An alternate scheme for attenuation compensation in photoacoustic tomography was proposed by Burgholzer et al. based on time reversal image reconstruction with a lossy wave equation.[38,39] In short, time reversal reconstruction works by running a numerical model of the acoustic forward problem backward in time. At each time step, the measured time-varying pressure signals are enforced (in time-reversed order) as a Dirichlet boundary condition at their recorded positions.[40,41] The initial pressure distribution is then recovered when t reaches 0. To compensate for acoustic attenuation, Burgholzer et al. used a numerical implementation of Stokes' lossy wave equation with the absorption term reversed in sign.[38] (Stokes' equation accounts for power law absorption of the form $\alpha = \alpha_0\omega^2$.) Reversing the attenuation term causes the acoustic waves in the numerical model to grow, rather than decay, as they

propagate back through the tissue. To keep noisy high-frequency signals from growing too quickly, the reconstruction was regularized by filtering the signals above a chosen cutoff frequency.

This approach was later extended by Treeby et al. to account for general power law absorption behavior using a lossy wave equation in which the absorption and dispersion are encapsulated by different terms.[6,19] The separation of the two allows the sign of the absorption term to be reversed to compensate for acoustic absorption, while leaving the sound speed dispersion term unchanged. The latter is important in time reversal attenuation compensation for recovering the correct shape of the propagating waves in dispersive media (i.e., when $y \neq 2$).[6] This approach has recently been used to compensate for acoustic attenuation in a number of pre-clinical imaging studies.[42–44] The compensation improves the resolution of the reconstructed images and allows deeper features to be visualized.[42] Huang et al. has also illustrated the applicability of this scheme to media with a heterogeneous distribution of acoustic absorption values.[45] This was demonstrated through a series of phantom measurements with pencil leads embedded in an agar phantom enclosed by an acrylic shell. The restriction of this approach to attenuation compensation is that time reversal must be used to reconstruct the image. For many canonical detector geometries, this may be less efficient than using other fast reconstruction algorithms.

2.3 Attenuation Compensation in Seismology

A remarkably similar problem to attenuation compensation in photoacoustic tomography exists in seismology, though it appears that this connection has not been previously explored. In seismology, the propagating seismic waves (generated by an explosive charge, for example) are attenuated due to scattering and absorption in the subsurface of the earth. This is accompanied by a velocity dispersion in which the different frequency components of the waves travel at different speeds. The strength and characteristics of the attenuation are normally quantified by a dimensionless parameter called the earth quality factor Q. This is related to the attenuation and dispersion in the medium via the equation[46]

$$Q(\omega) = \frac{1}{2}\left(\frac{|\omega|}{\alpha(\omega)c(\omega)} - \frac{\alpha(\omega)c(\omega)}{|\omega|}\right) \approx \frac{|\omega|}{2\alpha(\omega)c(\omega)}. \quad (6)$$

Different earth Q models are possible by choosing different forms for $\alpha(\omega)$ and $c(\omega)$. For example, the modified-Kolsky model assumes the attenuation is linearly dependent on frequency, with the attenuation and dispersion related via the Kramers-Kronig relations.[46] This is equivalent to the power law models discussed in Sec. 2.1, with the attenuation again dependent on both time and frequency.

Techniques for attenuation compensation in seismology (often referred to as inverse Q filtering) have a long history, and there is a considerable volume of associated literature (the monograph by Wang provides an excellent starting point for examining the seismic literature on attenuation compensation[46]). Most of these techniques fit into the framework of time-variant filtering. This allows the attenuated seismic traces (analogous to the recorded pressure signals in photoacoustics) to be corrected using a filter dependent on both time and frequency. The different compensation methods vary both in how the time-variant filter is constructed and in how it is applied. One of the simplest
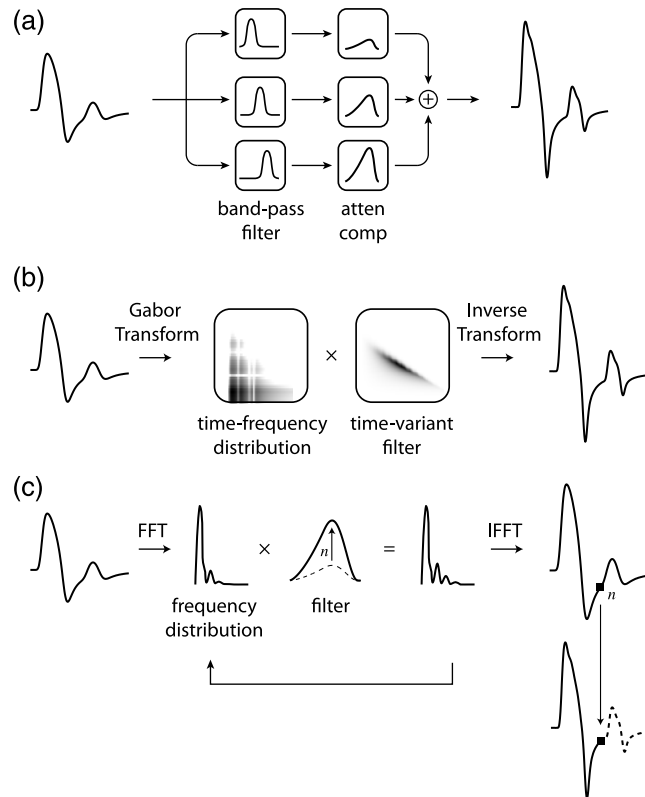

Fig. 1 Schematic of attenuation compensation techniques used in seismology: (a) time-variant spectral whitening (after Yilmaz[47]), (b) Gabor filtering, and (c) wave-field downward continuation.

approaches is called time-variant spectral whitening.[47] In this technique, the seismic trace is filtered using a series of narrow bandpass filters as shown in Fig. 1(a). Attenuation compensation is then performed separately for each frequency band, assuming the attenuation is frequency independent (where ω has a fixed value for each band). The final corrected signal is then obtained by recombining the filtered signals. If the features in the seismic trace can be assumed to be of a similar magnitude, this approach can also be used to estimate the amount of attenuation within each frequency band by fitting an envelope to the traces.[47]

Time-variant spectral whitening can be considered as a coarse method to decompose the seismic trace into a time-frequency distribution, which is then modified using a time-variant filter. A large number of extensions to this technique are therefore possible depending on how the time-frequency distribution and its inverse are constructed. For example, the Gabor transform (a particular type of short-time Fourier transform) has also been used for attenuation compensation in seismology.[48,49] The Gabor transform works by performing a series of localized Fourier transforms on the input signal using a moving time window. The resulting two-dimensional time-frequency representation of the signal can then be modified using a time-variant filter, as shown in Fig. 1(b). The filtered signal (in this case, the corrected seismic trace) is then recovered by performing an inverse Gabor transform.

An alternate way of applying the time-variant filter without explicitly decomposing the input signal into a time-frequency distribution is via wave-field downward continuation.[46] In this approach, the frequency spectrum of the seismic trace is multiplied by a frequency domain filter that corrects for acoustic
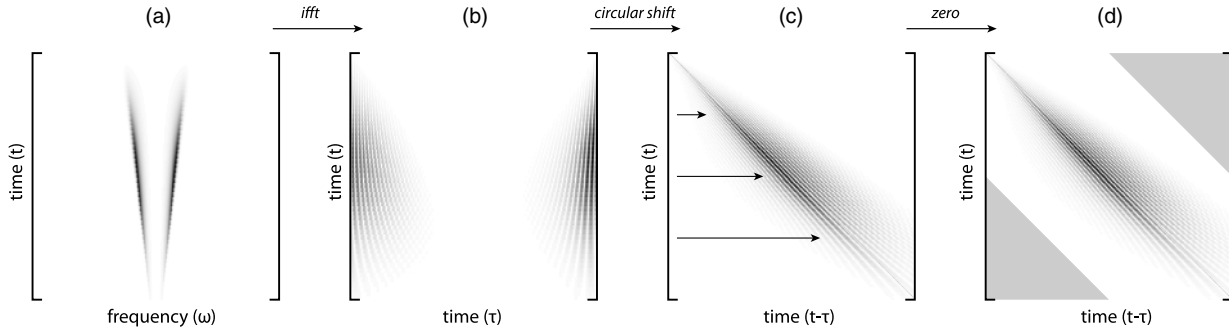
Fig. 2 Construction of a nonstationary convolution matrix used for time-variant filtering. (a) A frequency domain filter for each value of discrete time is constructed in the matrix rows. (b) The 1D inverse Fourier transform is performed along each matrix row to give the filter impulse response. (c) The rows are circular shifted (translated) based on their index, starting from 0. (d) The lower triangular part of the lower left quadrant and the upper triangular part of the upper right quadrant (shown in gray) are forced to be zero to make the filter acyclic.

attenuation assuming a particular discrete value of time or travel distance. In this case, the time is chosen to be $t = n\Delta t$, where $n = 0, 1, 2, \ldots, N - 1$, and Δt and N are chosen to match the acquisition settings. The resulting Fourier spectrum is then transformed back to the time-domain, and the n'th value of the signal is saved as the n'th value of the corrected time series. This procedure is repeated for each value of n, as shown in Fig. 1(c).

3 Attenuation Compensation Using Time-Variant Filtering

3.1 *Linear Time-Variant Filtering*

While many of the approaches for attenuation compensation in seismology may warrant further investigation into their applicability to photoacoustics, here we focus on a general method for time-variant filtering using a particular form of nonstationary convolution. This is formulated as an extension of stationary convolution where the filter is also allowed to vary as a function of output time (Margrave refers to this as nonstationary combination[50]). This can be expressed mathematically as

$$p_{\text{corr}}(t) = \int_{-\infty}^{\infty} F(t, t - \tau) p_{\text{att}}(\tau) d\tau, \qquad (7)$$

where $F(t, t - \tau)$ is the time-variant filter. In the stationary case, this would be replaced with $F(t - \tau)$. This expression is equivalent to a time-domain formulation of the wave-field downward continuation approach discussed in the previous section.[50] The advantage of allowing the filter to change as a function of output (rather than input) time is that the filter characteristics are able to change abruptly.[50] When expressed as a discrete matrix equation, Eq. (7) becomes

$$\begin{bmatrix} p_{\text{corr}}(t_1) \\ \vdots \\ p_{\text{corr}}(t_N) \end{bmatrix} = \begin{bmatrix} F(t_1, \tau_1) & \ldots & F(t_1, \tau_N) \\ \vdots & & \vdots \\ F(t_N, \tau_1) & \ldots & F(t_N, \tau_N) \end{bmatrix} \begin{bmatrix} p_{\text{att}}(\tau_1) \\ \vdots \\ p_{\text{att}}(\tau_N) \end{bmatrix}, \qquad (8)$$

where the attenuated and corrected pressure signals are given as column vectors of length N, and F is an $N \times N$ convolution matrix. In the stationary case, the convolution matrix is a Toeplitz matrix that can be formed by translating or shifting the impulse response of the filter based on the row index. In

the case of nonstationary convolution, the rows are shifted in the same way, but the impulse response is also allowed to vary from row to row. An intuitive way to construct the filter is as follows (see also Fig. 2):

a. Form an $N \times N$ matrix $F(t, \omega)$, where each row contains the desired frequency domain filter for the corresponding time index of the signal being filtered.

b. Compute the inverse Fourier transform over the matrix rows to yield the impulse response $F(t, \tau)$ of the time-variant filter. Note, if using a fast Fourier transform (FFT) algorithm that maps a complex domain input to a complex domain output (e.g., the `fft` function in MATLAB), the frequency domain filter constructed in Step (a) must contain both positive and negative frequencies in the correct order.

c. Circular shift (translate) each row in the matrix by the row index (starting from 0) to form the nonstationary convolution matrix $F(t, t - \tau)$.

d. Zero the lower triangular part of the lower left quadrant and the upper triangular part of the upper right quadrant to force the filter to be acyclic (see Fig. 2). In the stationary case, this is the equivalent of performing acyclic instead of circular convolution.

For attenuation compensation in photoacoustics, the time-variant filter F is constructed to counteract the effects of acoustic attenuation following a frequency power law as described by Eq. (5). This yields a filter of the form

$$F(t, \omega) = \exp\{\alpha_0 c_0 t[|\omega|^y - i \tan(\pi y/2)\omega|\omega|^{y-1}] W(t, \omega)\}. \qquad (9)$$

The $|\omega|^y$ term accounts for acoustic absorption, while the $\tan(\pi y/2)\omega|\omega|^{y-1}$ term accounts for sound speed dispersion. As the filter is applied directly to the recorded time-domain signals, both the absorption and dispersion terms are reversed in sign compared with Eq. (5) to counteract these effects in the forward problem. Note that the application of Eq. (9) via Eq. (8) is closely related to the attenuation compensation approach proposed by La Rivière et al.[29] Both multiply the recorded time signals by a coefficient matrix to correct for acoustic attenuation [see Sec. 2.2 and Eq. (14) in the Appendix]. However, in the case of time-variant filtering, the
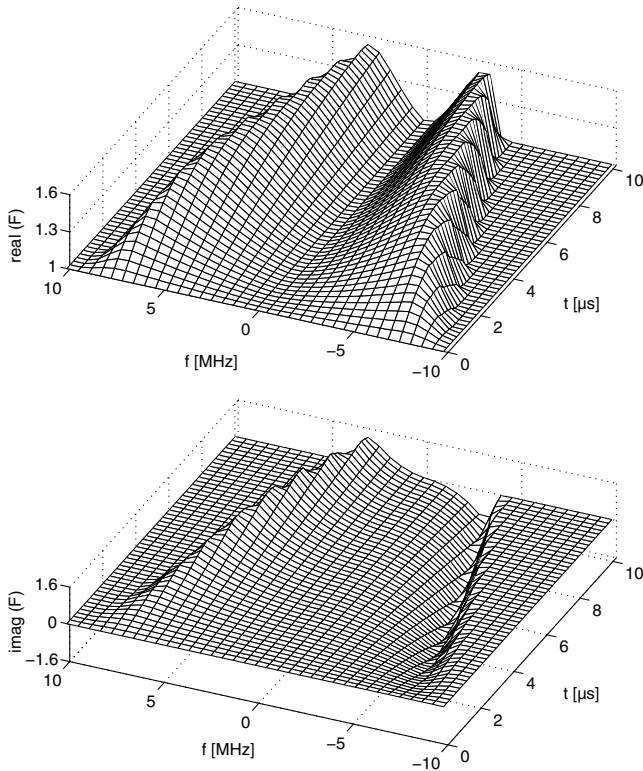
Fig. 3 Example of a time-variant filter $F(t, \omega)$ designed using Eq. (9) to compensate for acoustic attenuation in biological tissue where $c_0 = 1510$ ms^{-1}, $\alpha_0 = 5.5 \times 10^{-10}$ Np $(\text{rad/s})^{-y}$ m^{-1}, and $y = 1.5$ (here $\omega = 2\pi f$). The filter is regularized using a scaled Tukey window with a fixed taper ratio of 0.25 and a cutoff frequency varying from 10 MHz at $t = 0$ to 4 MHz at $t = 10$ μs.

coefficient matrix is formed as a filter within the framework of nonstationary convolution, rather than numerically computing the inverse of a coefficient matrix describing the forward problem.

The function $W(t, \omega)$ in Eq. (9) is a time-variant window used to regularize the filter. This is required to keep any high-frequency noise in the input signal from being amplified. Here the time-variant window is chosen to be a frequency domain Tukey or tapered cosine window for each discrete value of t. In other words, it consists of a series of scaled one-dimensional Tukey windows along each row of the convolution matrix. This choice allows the correct frequency dependence of the filter to be maintained within the flat component of the window (equivalent to a filter passband) while smoothly rolling off to zero at the cutoff frequency. An example of a time-variant filter constructed using Eq. (9) is shown in Fig. 3. In this case, the acoustic parameters are set to those of breast tissue, where $c_0 = 1510$ ms^{-1}, $\alpha_0 = 5.5 \times 10^{-10}$ Np $(\text{rad/s})^{-y}$ m^{-1} (equivalent to 0.75 dB MHz^{-y} cm^{-1}), and $y = 1.5$. The filter is regularized using a series of scaled Tukey windows with a fixed taper ratio of 0.25 and a cutoff frequency varying from 10 MHz at $t = 0$ to 4 MHz at $t = 10$ μs.

The computational complexity of applying the time-variant filter to a single time-domain signal is $O(N^2)$, where N is the number of time samples. The complexity of sequentially applying attenuation compensation to multiple signals is thus $O(MN^2)$, where M is the number of signals or detectors. This means the approach is computationally efficient, as the number of time samples in each recorded signal is typically small, even

for high-resolution images (e.g., $N = 500$ in Laufer et al.[43]). This restriction is because the required sampling frequency is ultimately limited by the bandwidth of the detectors, and the required acquisition time (or imaging depth) is ultimately limited by the sensitivity of the detectors and the penetration depth of the excitation laser light. In addition, the computational complexity of using time-variant filtering only grows linearly with the number of measurements or detectors, and this can be easily parallelized.

A simple example of using time-variant filtering to correct for acoustic attenuation and dispersion in a recorded time-domain signal is shown in Fig. 4. The forward signal was simulated using the second-order k-space model in the k-Wave MATLAB toolbox.[51,52] The initial photoacoustic pressure distribution was defined as two small discs and recorded by a point detector, as shown in Fig. 4(a). The recorded time signals for simulations in lossless (solid line) and lossy (dashed line) media without noise are shown in Fig. 4(b). The lossless signal is repeated in each panel for reference. Figure 4(c) shows the recorded signal after correction using a conventional time-invariant frequency domain filter of the form $e^{\alpha_0|\omega|^y d}$, equivalent to that used by Tan et al.[25] In this case, the propagation distance was fixed to $d = c_0 t$ where $t = 4$ μs. Since the filter characteristics do not depend on time, components of the signal arising from features shallower than the chosen distance have been overcorrected, and additional oscillations have been introduced. Figure 4(d) shows the recorded signal after correction using a time-variant filter based on Eq. (9) using only the absorption term (i.e., neglecting sound speed dispersion). In this case, the magnitude of the signal has been corrected, but components of the signal appear shifted due to the effects of sound speed dispersion. Figure 4(e) shows the time signal after correction using a time-variant filter based on Eq. (9) using both the absorption and dispersion terms. In this case, the corrected time signal closely matches the reference signal as desired. This illustrates the effectiveness of using time-variant filtering for attenuation compensation.

3.2 Adaptive Regularization Using Time-Frequency Analysis

In practice, the recorded photoacoustic time signals will always contain some level of noise. This means that any approach to attenuation compensation must include regularization to prevent noise at frequencies where the signal-to-noise ratio is low from being excessively amplified. In the case of time-variant filtering, the compensation is regularized by windowing the time-variant filter, as shown in Eq. (9). The choice of window shape and cutoff frequency is thus important for maintaining a balance between the fidelity of the compensation and the amount of noise introduced. In previous work on attenuation compensation using time reversal image reconstruction, regularization was achieved by filtering the absorption and dispersion terms in the governing equations using a Tukey window with a fixed cutoff frequency.[6] The cutoff frequency was chosen by examining where the average power spectrum of the recorded time signals reached the noise floor. A similar approach is possible using time-variant filtering by using a time-invariant window $W(\omega)$ with a fixed cutoff frequency. However, the use of time-variant filtering also introduces the possibility of selecting a time-variant window to regularize the compensation based on the local frequency content of the signal. This is significant, because high frequencies generated by deeper features in the tissue will
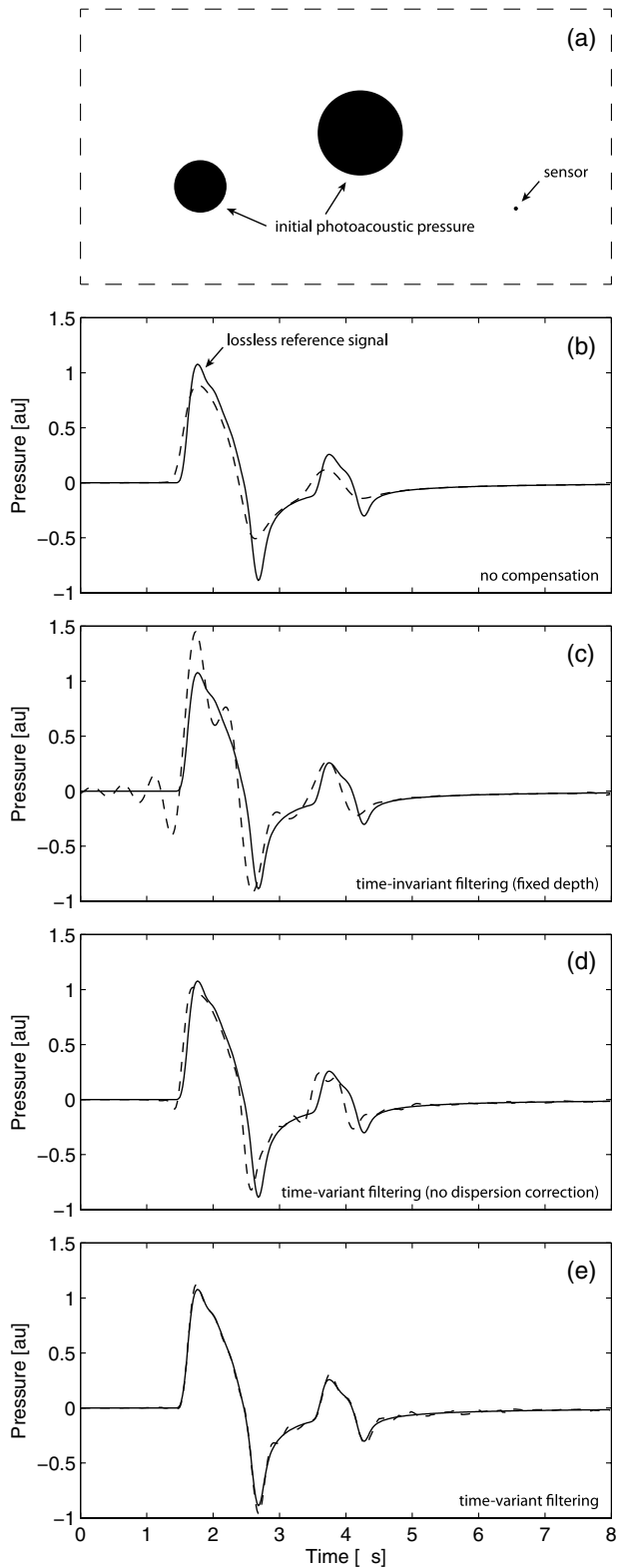
Fig. 4 Numerical example of using time-variant filtering to correct for acoustic attenuation and dispersion in a recorded time-domain signal. (a) Schematic of the simulation showing the initial pressure distribution and sensor. (b) The recorded time series in lossless (solid line) and lossy (dashed line) media. The lossless signal is repeated in each panel for reference. (c) Signal after correction using a time-invariant filter assuming a fixed distance (dashed line). (d) Signal after correction using a time-variant filter not accounting for sound speed dispersion (dashed line). (e) Signal after correction using a time-variant filter (dashed line).

undergo more attenuation before reaching the detector compared to shallow features (the waves have travelled further). This means that high-frequency components from shallow features (which appear early in the time signal) may be above the noise floor, while the same frequency components from deeper features (which appear later in the time signal) may not. The use of a time-variant window to regularize the attenuation compensation means the filter can adapt to the local frequency content of the recorded signal.

One approach to select the time-varying cutoff frequency for the window is to decompose each recorded time signal into a two-dimensional time-frequency distribution. There are many different ways to decompose a time-domain signal into such a distribution, each with different characteristics.[53] In this work, the time-frequency distribution is used only to select the cutoff frequency for the window, not to apply the time-variant filter like the Gabor filtering method discussed in Sec. 2.3, so the exact choice is not critical. A representative example is given in Fig. 5. The Shepp-Logan phantom[54] was used to define the initial photoacoustic pressure distribution analogous to Fig. 6 in Treeby et al.[6] The forward simulations were again computed in MATLAB using the k-Wave Toolbox. The computational domain was 1024×1024 grid points (52×52 mm, including a perfectly matched layer) supporting frequencies up to 14 MHz. The acoustic parameters were set to $c_0 = 1510 \text{ ms}^{-1}$, $\alpha_0 = 2.2 \times 10^{-9} \text{ Np (rad/s)}^{-y} \text{ m}^{-1}$, and $y = 1.5$. The signals were detected using a circle of 200 evenly distributed point detectors defined in Cartesian space with a radius of 25 mm. After the forward simulation, random Gaussian noise was added to the recorded signals to give a signal-to-noise ratio of 40 dB. The time signals recorded at one of the detector positions in both lossless (solid line) and lossy (dashed line) media are shown in Fig. 5(a). Three different time-frequency distributions of the lossy signal—the spectrogram, Wigner-Ville distribution, and Rihaczek distribution, respectively—are shown in Fig. 5(b)–5(d). Each distribution shows similar information on the local frequency content of the signal, but with different types and levels of artifacts (a detailed discussion of the merits of different time-frequency distributions is given by Boashash[53]).

For the simulations presented here, the Rihaczek distribution was used to derive the time-variant cutoff frequency (other distributions could similarly be used if desired). The two-dimensional Rihaczek distribution $R_z(t, f)$ of a time-varying signal $s(t)$ is calculated by $R_z(t, f) = s(t)S^*(f)e^{-i2\pi ft}$, where $S^*(f)$ is the complex conjugate of the Fourier transform of $s(t)$.[53] Given this distribution, the cutoff frequency for each discrete time-point was selected as the frequency at which a particular percentage of the total energy was reached, in this case 98% (this was chosen heuristically). The variation in the cutoff frequency over time was then smoothed using a piecewise constant cubic spline. The resulting time-varying cutoff frequency for the signal shown in Fig. 5(a) is given as the white dashed line in Fig. 5(d). The corrected time signal after applying the filter is shown in Fig. 5(e).

The reconstructed photoacoustic images of the Shepp-Logan phantom are shown in Fig. 6. The recorded signals were first interpolated onto a continuous circular sensor surface using linear interpolation[52] and then reconstructed using time reversal (any applicable reconstruction algorithm could similarly be used). The reconstructed image without attenuation compensation is shown in Fig. 6(a). A one-dimensional profile through $x = 0$ is shown in Fig. 6(b), with the corresponding profile
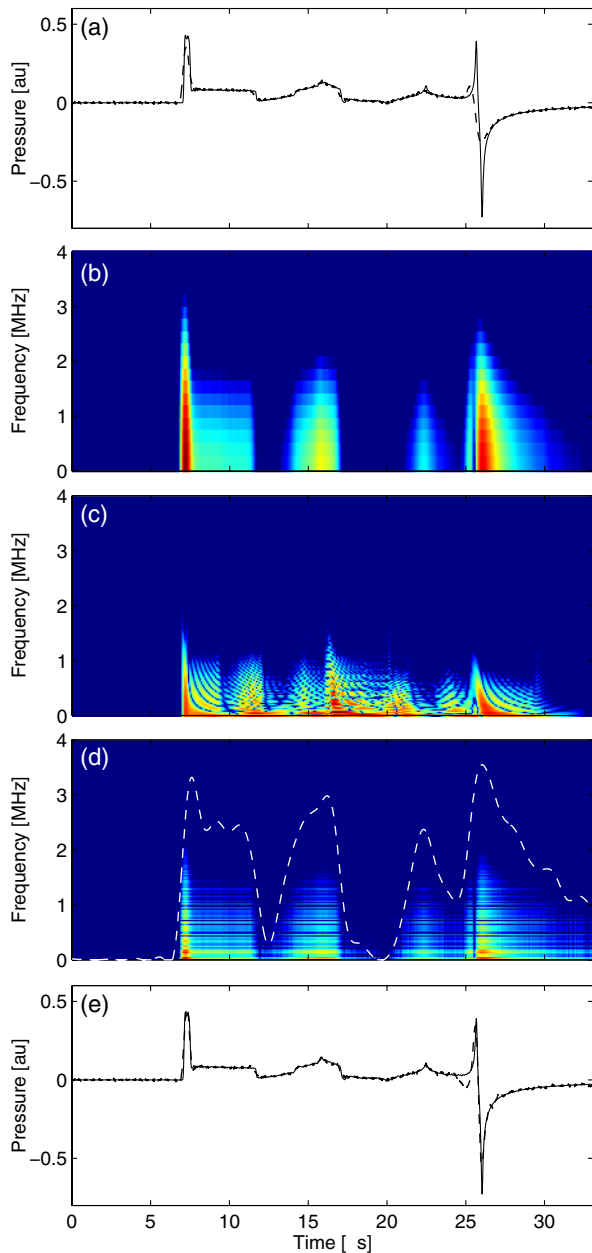
Fig. 5 Attenuation compensation using time-variant filtering. (a) Example of a time series recorded in a lossy medium (dashed line) against the equivalent signal recorded in a lossless medium (solid line) for an initial photoacoustic pressure distribution defined by the Shepp-Logan phantom. (b) Spectrogram time-frequency distribution of the recorded time signal. (c) Wigner-Ville time-frequency distribution of the recorded signal. (d) Rihaczek time-frequency distribution of the recorded signal. The extracted time-variant cutoff frequency is shown with a dashed white line. (e) Corrected time signal (dashed line) after time-variant filtering.

through the initial photoacoustic pressure distribution shown with a light line. The acoustic attenuation has blurred the edges of the reconstructed image, and the overall magnitude of the image features has been reduced. The image reconstructed after attenuation compensation using time-variant filtering is shown in Fig. 6(c) and 6(d). The filter matrix was constructed using Eq. (9), with the time-varying cutoff frequency for each recorded signal chosen separately based on the Rihaczek time-frequency distribution of each signal. The sharpness of

the reconstructed image compared to the uncompensated case is considerably improved, and the reconstructed pressure magnitudes are much closer to quantitatively accurate values. Due to the band-limited frequency response of the recorded signals (some high frequencies are below the noise floor when the acoustic waves reach the detector), the compensation cannot completely recover the frequency content of the initial pressure distribution. This results in a small amount of overshoot (Gibbs phenomenon) near the sharp edges in the image.

The corresponding reconstruction using the *average* time-frequency distribution of all the recorded signals to select the cutoff frequency for the window is shown in Fig. 6(e) and 6(f). Using the average time-frequency distribution to construct the filter and then applying the same filter to all of the time signals is considerably faster than constructing and applying different filters for each signal. The difference is due to the computational cost of creating each nonstationary convolution matrix as described in Sec. 3.1. Again, the sharpness and magnitude of the reconstructed image are considerably improved relative to the uncompensated case. Using the individual filters gives a marginally sharper image as seen in Fig. 6(c) and 6(d). However, this comes at the expense of an increase in compensation time as mentioned above. For comparison, the reconstruction after attenuation compensation using time-variant filtering with a fixed cutoff frequency of 3 MHz is shown in Fig. 6(g) and 6(h). Using a fixed cutoff frequency is similar to using time reversal reconstruction with attenuation compensation, which is also regularized by a single cutoff frequency (see Fig. 6(e) of Treeby et al.[6] for comparison). In this case, the edges of the reconstructed image appear sharp, but significantly more noise has been introduced. This is because the same cutoff frequency is used regardless of the local frequency content of the recorded time-domain signals.

4   Application to Experimental Data

To demonstrate the applicability of attenuation compensation via time-variant filtering in a practical setting, the method was applied to an experimental photoacoustic dataset of the abdomen of a pregnant female mouse. The dataset was taken from Laufer et al.[44] and was acquired using a planar tomography system based on a high-sensitivity Fabry-Perot sensor.[55] A detailed description of the experimental protocol and hardware is given in these references and is not repeated here. The dataset was acquired using a planar scan area of 16×16 mm with a step size of 115 μm and contained a total of 19,881 waveforms, each trimmed to 300 time points. The images were reconstructed using time reversal image reconstruction via the k-Wave toolbox,[52] with the sound speed selected based on an autofocus approach.[56] After reconstruction, a first-order correction for the optical attenuation in tissue was also applied, where $p_{corrected} = p_{reconstructed} \times e^{\mu_{eff} z}$. Here, z corresponds to the distance in the depth direction, and a value of $\mu_{eff} = 0.1$ cm^{-1} was used for the effective scattering coefficient.

The reconstructed images with and without attenuation compensation are shown in Fig. 7. The top two panels in each plot correspond to maximum intensity projections (MIPs) through the depth and lateral dimensions of the reconstructed three-dimensional image. The bottom panel shows a one-dimensional profile through the lateral MIP at $y = 8.5$ mm. The location of the profile in the lateral MIP is shown with a dashed white line. The images show the superficial vasculature in the skin of the parent mouse along with the developing rib cage and organs of
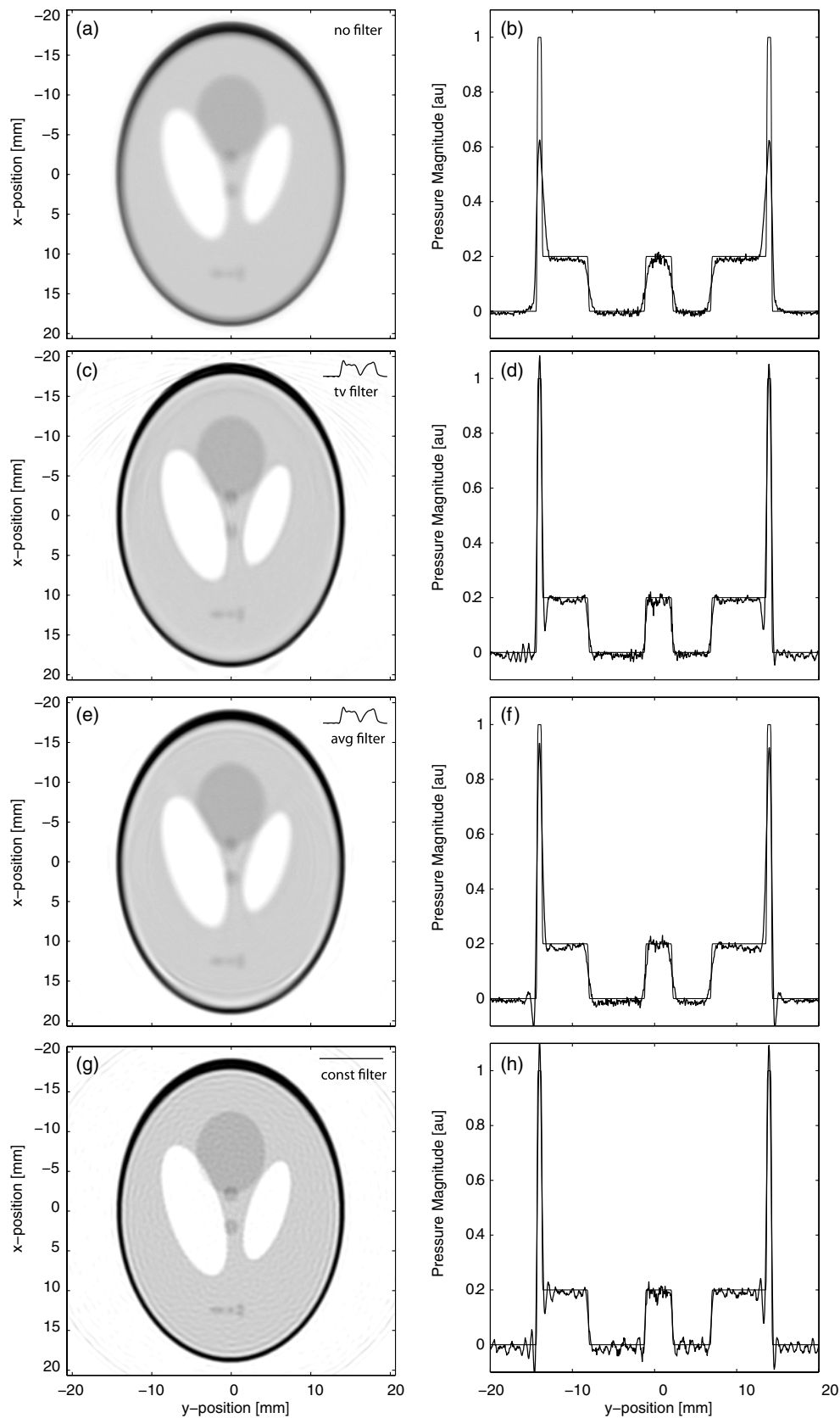
Fig. 6 Effect of using time-variant filtering to correct for acoustic attenuation on reconstructed images of the Shepp-Logan phantom. (a) Reconstruction with no compensation for acoustic attenuation. (b) Profile through $x = 0$. The equivalent profile through the initial pressure distribution is shown with a light line for reference. (c) Reconstruction after time-variant filtering using a cutoff frequency chosen separately for each recorded signal based on the individual time-frequency distributions. (d) Profile through $x = 0$. (e) Reconstruction after time-variant filtering using a cutoff frequency derived from the average time-frequency distribution of all the recorded signals. (f) Profile through $x = 0$. (g) Reconstruction after time-variant filtering using a fixed cutoff frequency of 3 MHz. (h) Profile through $x = 0$.
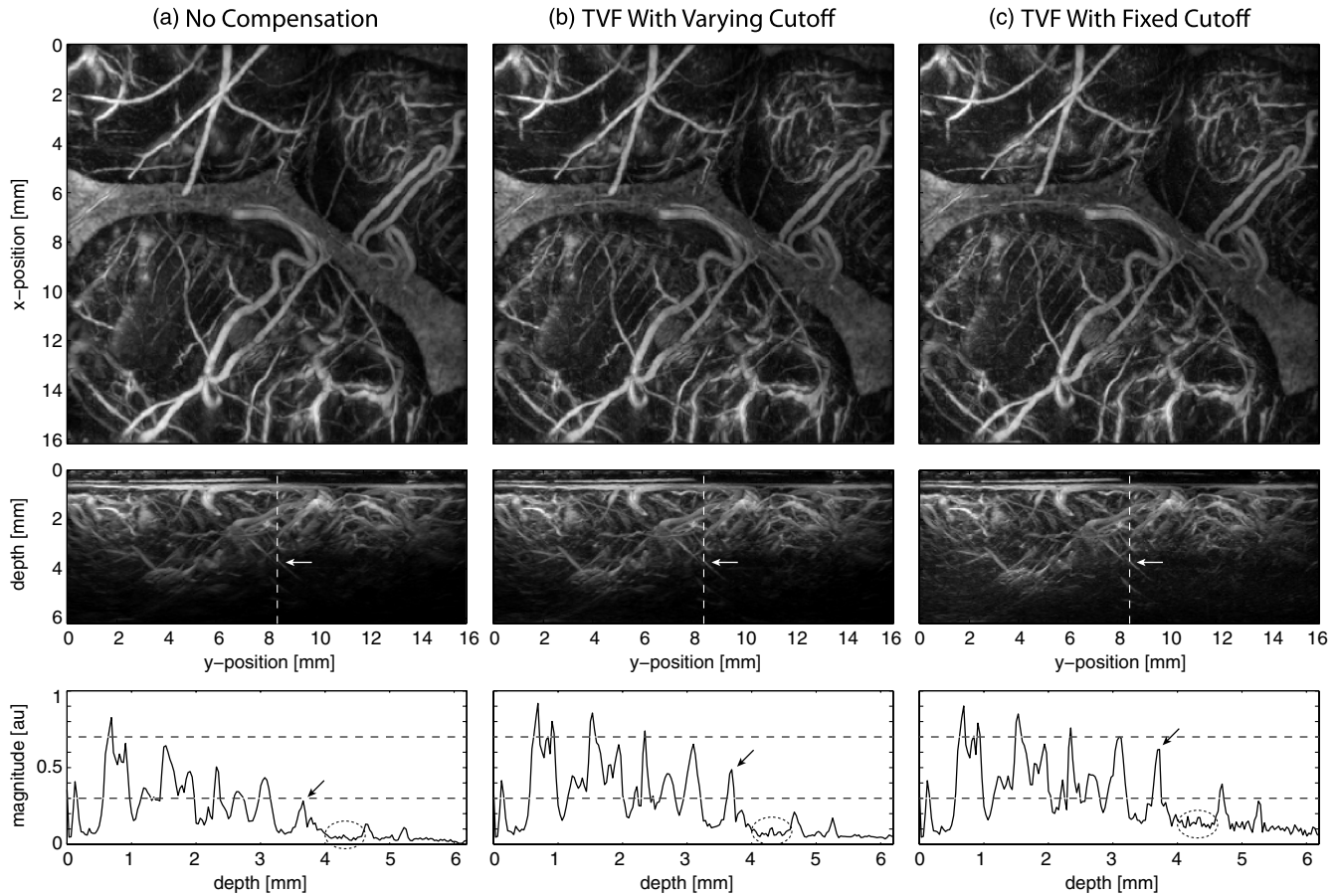
Fig. 7 Application of attenuation compensation using time-variant filtering to an experimental dataset of the vascular networks in the abdomen of a pregnant female mouse. (a) Reconstruction without compensation for acoustic attenuation. (b) Reconstruction including compensation for acoustic attenuation using a window with a time-varying cutoff frequency derived from the average time-frequency distribution of the recorded signals. (c) Reconstruction including compensation for acoustic attenuation using a window with a fixed cutoff frequency of 20 MHz. The three panels in each image correspond to maximum intensity projections (MIPs) through the depth and lateral directions and a one-dimensional profile through the lateral MIP at $y = 8.5$ mm. The location of the profile in the lateral MIP is shown with a dashed white line. The arrows indicate illustrative features to compare the three reconstructions.

two embryos.[44] Figure 7(b) shows the image reconstructed after applying attenuation compensation to the recorded time signals using time-variant filtering. The filter matrix was constructed using Eq. (9), with the time-varying cutoff frequency for the window derived from the average time-frequency distribution of the recorded signals (shown in Fig. 8). The attenuation parameters were set to those of breast tissue, where $\alpha_0 = 5.5 \times 10^{-10}$ Np $(\text{rad/s})^{-y}$ m^{-1}, and $y = 1.5$. Using a standard desktop computer with a four-core Intel Core i7 950 processor, constructing the time-variant filter using the average Rihaczek time-frequency distribution in MATLAB took approximately 4 s, while applying the filter to the 19,881 recorded waveforms using matrix multiplication took approximately 0.2 s. Figure 7(c) shows the image reconstructed after applying attenuation compensation via time-variant filtering with a fixed window cutoff frequency of 20 MHz.

When attenuation compensation is included, the edges of the superficial blood vessels are sharpened, and the visibility of the deeper vessels is significantly improved. As an illustrative example, the magnitude of the vessel denoted by the arrows has been noticeably increased, while the corresponding full width at half maximum (relative to the noise floor) has been reduced. Compared to using a time-varying cutoff frequency for the filter window, the use of a fixed cutoff frequency of 20 MHz has further
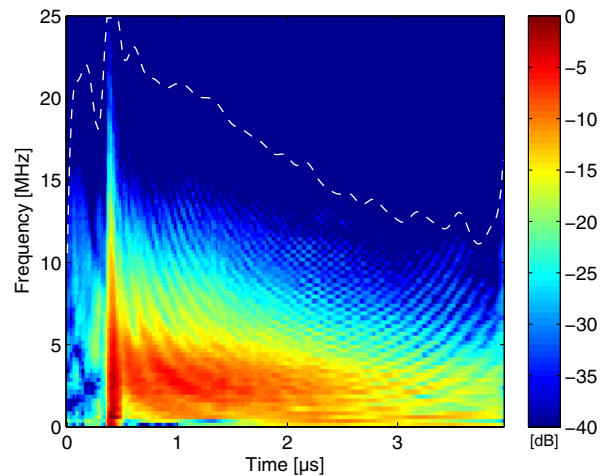

Fig. 8 Average time-frequency distribution of the recorded time-domain pressure signals for the photoacoustic image shown in Fig. 7. The extracted time-varying cutoff frequency is shown with a dashed white line.

increased the magnitude of some of the deeper features in the image (see Fig. 8 for a comparison of the cutoff frequencies and the average time-frequency distribution of the recorded signals). However, this increase comes at the expense of introducing additional noise into the reconstructed image. This is particularly noticeable at greater depths, for example, in the noise floor shown in the one-dimensional profiles in Fig. 7 (dashed circles).

Compared to attenuation compensation using time reversal,[6,42] the use of time-variant filtering has several notable advantages. First, it applies directly to the recorded time-domain signals and can thus be used with any detector geometry or reconstruction algorithm. Second, a time-variant window can be used to regularize the compensation. This allows the compensation to adapt to the local frequency content of the recorded signals at different times or travel distances, and minimizes the amount of noise introduced. On the other hand, attenuation compensation using time reversal allows the absorption coefficient to be spatially varying, which is not possible with time-variant filtering.[45] This may be important for strongly heterogeneous media, for example, photoacoustic imaging of the brain, where the generated waves must also travel through the skull,[57] or if the detectors are connected to the sample via a coupling medium such as water with different acoustic properties.

5 Conclusion

A new method for attenuation compensation in photoacoustic tomography using time-variant filtering is presented. The compensation is applied using an extension of stationary convolution, where the convolution matrix or filter is allowed to vary as a function of output time as well as frequency. This enables a two-dimensional filter to be constructed to correct for acoustic attenuation and dispersion following a frequency power law. Regularization is achieved using a time-variant frequency domain Tukey window, where the cutoff frequency is chosen based on the local time-frequency distribution of the recorded signals. Compared to selecting a fixed cutoff frequency, this reduces the amount of high-frequency noise introduced. After construction, the time-variant filter (or convolution matrix) is applied directly to the recorded time-domain signals using matrix multiplication. The approach is very general and can be used in combination with any detector geometry or image reconstruction algorithm. Moreover, the time-variant filter can be constructed and applied to a complete photoacoustic dataset within a few seconds using a standard computer. As with previous studies, when compensation for acoustic attenuation is used, a general improvement in image magnitude and resolution is seen, particularly for features at greater depths. This is of particular importance in the context of quantitative imaging.[3] Overall, time-variant filtering provides a general, fast, and robust way to compensate for acoustic attenuation in photoacoustic tomography under the assumption that the distribution of attenuation parameters within the medium is homogenous. Future work will consider optimizing the performance of the time-variant window used for regularization. MATLAB codes to perform attenuation compensation via time-variant filtering will be made freely available as part of the open-source k-Wave Toolbox (http://www.k-wave.org).

Appendix: La Rivière approach

Following La Rivière et al. and Ammari et al.,[29,33] the photoacoustic wave equation given an initial pressure distribution $p_0(x)$ at time $t = t_0$ can be written in the form

$$\left(\nabla^2 - \frac{1}{c_0^2}\frac{\partial^2}{\partial t^2}\right)p(x,t) = -\frac{p_0(x)}{c_0^2}\frac{\partial}{\partial t}\delta(t - t_0). \quad (10)$$

Taking the temporal Fourier transform using the conventions given in Morse and Ingard[58] and assuming $t_0 = 0$ then gives

$$\left(\nabla^2 + \frac{\omega^2}{c_0^2}\right)p(x,\omega) = -\frac{p_0(x)}{c_0^2}\frac{i\omega}{2\pi}. \quad (11)$$

Using Eq. (4), the equivalent relation for the lossy case is

$$[\nabla^2 + k^2(\omega)]p_{\mathrm{att}}(x,\omega) = -\frac{p_0(x)}{c_0^2}\frac{i\omega}{2\pi}. \quad (12)$$

The attenuated and lossless pressures $p_{att}(x,\omega)$ and $p(x,\omega)$ can thus be related by

$$p_{\mathrm{att}}(x,\omega) = \frac{\omega}{k(\omega)c_0}p\Big(x, k(\omega)c_0\Big), \quad (13)$$

where $p(x, k(\omega)c_0) = \int p(x,t)e^{ik(\omega)c_0 t}\mathrm{d}t$. This expression can be written as an integral equation

$$p_{\mathrm{att}}(x,t) = \int\frac{\omega}{k(\omega)c_0}e^{-i\omega t}\int p(x,t)e^{ik(\omega)c_0 t}\mathrm{d}t\mathrm{d}\omega, \quad (14)$$

which can be formed as a discrete matrix equation and inverted numerically. La Rivière et al. used an equation of this form with $k(\omega) = \omega/c(\omega) + i\alpha_0|\omega|$, where the dispersion relation is based on Szabo's equation for $y = 1$.[28,29]

References

1. M. Xu and L. V. Wang, "Photoacoustic imaging in biomedicine," *Rev. Sci. Instrum.* **77**(4), 041101 (2006).
2. P. Beard, "Biomedical photoacoustic imaging," *Interface Focus* **1**(4), 602–631 (2011).
3. B. Cox et al., "Quantitative spectroscopic photoacoustic imaging: a review," *J. Biomed. Opt.* **17**(6), 061202 (2012).
4. P. Kuchment and L. Kunyansky, "Mathematics of thermoacoustic tomography," *Eur. J. Appl. Math.* **19**(02), 191–224 (2008).
5. G. Ku et al., "Multiple-bandwidth photoacoustic tomography," *Phys. Med. Biol.* **49**(7), 1329–1338 (2004).
6. B. E. Treeby, E. Z. Zhang, and B. T. Cox, "Photoacoustic tomography in absorbing acoustic media using time reversal," *Inverse Probl.* **26**(11), 115003 (2010).
7. A. B. Bhatia, *Ultrasonic Absorption: An Introduction to the Theory of Sound Absorption and Dispersion in Gases, Liquids, and Solids*, Dover Publications, New York (1985).
8. B. E. Treeby et al., "Measurement of the ultrasound attenuation and dispersion in whole human blood and its components from 0–70 MHz," *Ultrasound Med. Biol.* **37**(2), 289–300 (2011).
9. M. E. Lyons and K. J. Parker, "Absorption and attenuation in soft tissues II—Experimental results," *IEEE Trans. Ultrason. Ferroelectr. Freq. Control* **35**(4), 511–521 (1988).

10. B. I. Raju and M. A. Srinivasan, "High-frequency ultrasonic attenuation and backscatter coefficients of *in vivo* normal human dermis and subcutaneous fat," *Ultrasound Med. Biol.* **27**(11), 1543–1556 (2001).

11. F. A. Duck, *Physical Properties of Tissue: A Comprehensive Reference Book*, Academic Press, San Diego (1990).

12. R. Esenaliev et al., "Axial resolution of laser optoacoustic imaging: influence of acoustic attenuation and diffraction," *Proc. SPIE* **3254**, 294–306 (1998).

13. S. K. Patch and M. Haltmeier, "Thermoacoustic tomography—Ultrasound attenuation artifacts," in *Proc. IEEE Nuclear Science Symposium Conference*, San Diego, CA, pp. 2604–2606, IEEE (2006).

14. B. E. Treeby and B. T. Cox, "Fast tissue-realistic models of photoacoustic wave propagation for homogeneous attenuating media," *Proc. SPIE* **7177**, 717716 (2009).

15. X. L. Deán-Ben, D. Razansky, and V. Ntziachristos, "The effects of acoustic attenuation in optoacoustic signals," *Phys. Med. Biol.* **56**(18), 6129–6148 (2011).

16. H. Roitner et al., "Experimental evaluation of time domain models for ultrasound attenuation losses in photoacoustic imaging," *J. Acoust. Soc. Am.* **131**(5), 3763–3774 (2012).

17. P. J. La Riviere, J. Zhang, and M. A. Anastasio, "Ultrasonic attenuation correction in optoacoustic tomography," *Proc. SPIE* **6086**, 69861I (2006).

18. B. T. Cox, J. G. Laufer, and P. C. Beard, "The challenges for quantitative photoacoustic imaging," *Proc. SPIE* **7177**, 717713 (2009).

19. B. E. Treeby and B. T. Cox, "Modeling power law absorption and dispersion for acoustic propagation using the fractional Laplacian," *J. Acoust. Soc. Am.* **127**(5), 2741–2748 (2010).

20. K. Waters, J. Mobley, and J. Miller, "Causality-imposed (Kramers-Kronig) relationships between attenuation and dispersion," *IEEE Trans. Ultrason. Ferroelectr. Freq. Control* **52**(5), 822–823 (2005).

21. K. R. Waters et al., "On the applicability of Kramers-Kronig relations for ultrasonic attenuation obeying a frequency power law," *J. Acoust. Soc. Am.* **108**(2), 556–563 (2000).

22. J. F. Kelly, R. J. McGough, and M. M. Meerschaert, "Analytical time-domain Green's functions for power-law media," *J. Acoust. Soc. Am.* **124**(5), 2861–2872 (2008).

23. T. L. Szabo, "Time domain wave equations for lossy media obeying a frequency power law," *J. Acoust. Soc. Am.* **96**(1), 491–500 (1994).

24. W. Chen and S. Holm, "Modified Szabos wave equation models for lossy media obeying frequency power law," *J. Acoust. Soc. Am.* **114**(5), 2570–2574 (2003).

25. Y. Tan et al., "Photoacoustic imaging with attenuation rectification of different frequent components of photoacoustic signal," *Proc. SPIE* **5630**, 668–674 (2005).

26. X. L. Deán-Ben, D. Razansky, and V. Ntziachristos, "Correction for acoustic attenuation effects in optoacoustic tomographic reconstructions," *Proc. SPIE* **8090**, 809014 (2011).

27. J. Bauer-Marschallinger et al., "Ultrasonic attenuation of biomaterials for compensation in photoacoustic imaging," *Proc. SPIE* **7899**, 789931 (2011).

28. P. J. La Riviere, J. Zhang, and M. A. Anastasio, "Image reconstruction in optoacoustic tomography accounting for frequency-dependent attenuation," in *Proc. IEEE Nuclear Science Symposium Conference*, Las Croabas, Puerto Rico, pp. 1841–1845, IEEE (2005).

29. P. J. La Riviere, J. Zhang, and M. A. Anastasio, "Image reconstruction in optoacoustic tomography for dispersive acoustic media," *Opt. Lett.* **31**(6), 781–783 (2006).

30. N. V. Sushilov and R. S. C. Cobbold, "Frequency-domain wave equation and its time-domain solutions in attenuating media," *J. Acoust. Soc. Am.* **115**(4), 1431–1436 (2004).

31. H. Roitner and P. Burgholzer, "Efficient modeling and compensation of ultrasound attenuation losses in photoacoustic imaging," *Inverse Probl.* **27**(1), 015003 (2011).

32. R. Kowar and O. Scherzer, "Attenuation models in photoacoustics," in *Mathematical Modeling in Biomedical Imaging II: Optical, Ultrasound, and Opto-Acoustic Tomographies*, H. Ammari, Ed., Lecture Notes in Mathematics, Vol. 2035, pp. 85–129, Springer-Verlag, Berlin (2012).

33. H. Ammari et al., "Photoacoustic imaging for attenuating acoustic media," in *Mathematical Modeling in Biomedical Imaging II: Optical, Ultrasound, and Opto-Acoustic Tomographies*, H. Ammari, Ed., Lecture Notes in Mathematics, Vol. 2035, pp. 57–84, Springer-Verlag, Berlin (2012).

34. D. Modgil and P. J. La Riviere, "Photoacoustic image reconstruction in an attenuating medium using singular value decomposition," in *Proc. IEEE Nuclear Science Symposium Conference*, Dresden, Germany, pp. 4489–4493, IEEE (2008).

35. D. Modgil, M. A. Anastasio, and P. J. La Riviere, "Photoacoustic image reconstruction in an attenuating medium using singular value decomposition," *Proc. SPIE* **7177**, 71771B (2009).

36. D. Modgil, B. E. Treeby, and P. J. La Riviere, "Photoacoustic image reconstruction in an attenuating medium using singular-value decomposition," *J. Biomed. Opt.* **17**(6), 061204 (2012).

37. R. Kowar, "Integral equation models for thermoacoustic imaging of acoustic dissipative tissue," *Inverse Probl.* **26**(9), 095005 (2010).

38. P. Burgholzer et al., "Compensation of acoustic attenuation for high-resolution photoacoustic imaging with line detectors," *Proc. SPIE* **6437**, 643724 (2007).

39. P. Burgholzer et al., "Information changes and time reversal for diffusion-related periodic fields," *Proc. SPIE* **7177**, 717723 (2009).

40. Y. Xu and L. V. Wang, "Time reversal and its application to tomography with diffracting sources," *Phys. Rev. Lett.* **92**(3), 033902 (2004).

41. D. Finch and S. K. Patch, "Determining a function from its mean values over a family of spheres," *SIAM J. Math Anal.* **35**(5), 1213–1240 (2004).

42. B. E. Treeby et al., "Acoustic attenuation compensation in photoacoustic tomography: application to high-resolution 3D imaging of vascular networks in mice," *Proc. SPIE* **7899**, 78992Y (2011).

43. J. Laufer et al., "*In vivo* preclinical photoacoustic imaging of tumor vasculature development and therapy," *J. Biomed. Opt.* **17**(5), 056016 (2012).

44. J. Laufer et al., "*In vivo* photoacoustic imaging of mouse embryos," *J. Biomed. Opt.* **17**(6), 061220 (2012).

45. C. Huang et al., "Photoacoustic computed tomography correcting for heterogeneity and attenuation," *J. Biomed. Opt.* **17**(6), 061211 (2012).

46. Y. Wang, *Seismic Inverse Q Filtering*, Blackwell Publishing, Oxford (2008).

47. O. Yilmaz, *Seismic Data Analysis: Processing, Inversion, and Interpretation of Seismic Data*, Society of Exploration Geophysicists, Tulsa (2001).

48. Y. Wang, "Inverse Q-filter for seismic resolution enhancement," *Geophysics* **71**(3), V51–V60 (2006).

49. G. F. Margrave, M. P. Lamoureux, and D. C. Henley, "Gabor deconvolution: estimating reflectivity by nonstationary deconvolution of seismic data," *Geophysics* **76**(3), W15–W30 (2011).

50. G. F. Margrave, "Theory of nonstationary linear filtering in the Fourier domain with application to time-variant filtering," *Geophysics* **63**(1), 244–259 (1998).

51. B. E. Treeby and B. T. Cox, "A k-space Greens function solution for acoustic initial value problems in homogeneous media with power law absorption," *J. Acoust. Soc. Am.* **129**(6), 3652–3660 (2011).

52. B. E. Treeby and B. T. Cox, "k-Wave: MATLAB toolbox for the simulation and reconstruction of photoacoustic wave fields," *J. Biomed. Opt.* **15**(2), 021314 (2010).

53. B. Boashash, *Time-Frequency Signal Analysis and Processing: A Comprehensive Reference*, Elsevier, Oxford (2003).

54. L. A. Shepp and B. F. Logan, "Reconstructing interior head tissue from x-ray transmissions," *IEEE Trans. Nucl. Sci.* **21**(1), 228–236 (1974).

55. E. Zhang, J. Laufer, and P. Beard, "Backward-mode multiwavelength photoacoustic scanner using a planar Fabry-Perot polymer film ultrasound sensor for high-resolution three-dimensional imaging of biological tissues," *Appl. Opt.* **47**(4), 561–577 (2008).

56. B. E. Treeby et al., "Automatic sound speed selection in photoacoustic image reconstruction using an autofocus approach," *J. Biomed. Opt.* **16**(9), 090501 (2011).

57. C. Huang et al., "Aberration correction for transcranial photoacoustic tomography of primates employing adjunct image data," *J. Biomed. Opt.* **17**(6), 066016 (2012).

58. P. M. Morse and K. U. Ingard, *Theoretical Acoustics*, Princeton University Press, Princeton, New Jersey (1968).